Channel Tracking for Rake Receivers in Closely Spaced Multipath Environments

Gunnar Fock, Jens Baltersee, Peter Schulz-Rittich, and Heinrich Meyr, *Fellow, IEEE*

***Abstract*—This paper deals with the problem of channel tracking for RAKE receivers in propagation environments characterized by closely spaced multipath components. After outlining why conventional single-path channel tracking algorithms fail in such scenarios, several new estimation algorithms are developed that are tailored to channels with closely spaced multipaths. This is achieved by removing or minimizing self-interference caused by multipath components. Other interfering users are treated as noise. Both timing tracking and phasor tracking and their interaction are covered in this paper. The derived algorithms are benchmarked against perfect channel knowledge on one hand and conventional tracking algorithms on the other hand, both in a UMTS test scenario. In moderate scenarios, the use of these new algorithms leads to performance improvements of up to 2 dB, in terms of signal-to-noise ratio (SNR) at moderate bit error rates, and even manages to track the channel in conditions where conventional tracking algorithms fail completely.**

***Index Terms*—Delay estimation, interference suppression, multipath channels, phase estimation, synchronization.**

I. Introduction

THE APPLICATION of code-division multiple access (CDMA) in communication systems has gained tremendous attention during the development of the third-generation (3G) standards and has become part of several of the new standards belonging to the 3G family. Despite the fact that advanced techniques like multiuser detection can largely boost the overall performance of a CDMA system, the RAKE is still the receiver structure of choice for the first round of low-complexity receivers for 3G systems. Moreover, the RAKE is also the basic building block of more complex receiver structures employing serial or parallel multiuser interference cancellation. Since the performance of the RAKE is very much dependent on the quality of its channel estimates, it is extremely important to provide the RAKE with accurate channel estimates. In the case of a distinct multipath channel profile, this is achieved by estimating multipath delays and fading coefficients. The two corresponding tasks, timing and phasor estimation, are the topic of this paper. For the case of a single fading path, there is a wide variety of algorithms that are capable of this task including the "standard" early–late timing error detector. But these algorithms suffer from severe performance degradation or even complete failure if the channel is frequency selective and there are more than one multipath components close to each other [4], [16].

This paper models the conventional tracking approach in conjunction with the multipath channel and outlines why and how the conventional approach fails. Starting with this knowledge, algorithms are developed that can cope with multipath scenarios. There are two possible approaches to deal with this problem: one can be characterized as interference cancellation, which was described independently in [13] and in [14]. The interference cancellation scheme described in Section III-B of this paper is based on the last reference. In both of the references and in this paper, the interference cancellation is performed after the timing error detector (TED) and not before, as in [5], where as a result excessive signal processing is needed. A similar way of dealing with interference cancellation is also described in [6], which, however, cannot track data modulated signals. The second approach can be classified as interference minimization [15]. Both approaches can be applied to timing tracking, whereas for phasor estimation, only an interference minimization scheme is applicable. At the end of this paper, the new algorithms are benchmarked in comparison to the conventional ones and to the bound of perfect channel knowledge. These benchmark tests are conducted in a universal mobile telecommunications service (UMTS) test environment.

II. System Model

The system we are concerned with consists of a CDMA transmitter sending a complex valued data sequence $\{a_n\}$. These data symbols are spread by the spreading factor N_c using the effective spreading sequence $\{d_\nu\}$, which is assumed to be complex valued as well. This spreading sequence can have a periodicity much larger than the symbol duration. (The same techniques described here may be applied to different spreading schemes if the corresponding despreading scheme is adapted appropriately.) The spread sequence is transmitted using a pulse shaping filter $g(t)$, which in the case of Third-Generation Partnership Program (3GPP) [9] is a root-raised cosine filter with a rolloff factor of 0.22. The resulting baseband-equivalent transmit signal is given by

$$s(t) = \sum_n a_n \sum_{\nu=0}^{N_c-1} d_\nu g(t - nT - \nu T_c) \tag{1}$$

where T denotes the symbol duration and T_c is the chip duration. To incorporate effective spreading sequences with a periodicity longer than one symbol (e.g., resulting from additional scrambling), d_ν is now replaced by $d_{nN_c+\nu}$. The signal from the

Manuscript received January 25, 2001; revised June 13, 2001. This work was supported by Agere Systems.

The authors are with the Integrated Systems for Signal Processing Laboratory, Aachen University of Technology (RWTH), Aachen, Germany (e-mail: fock@iss.rwth-aachen.de).

Publisher Item Identifier S 0733-8716(01)10301-X.

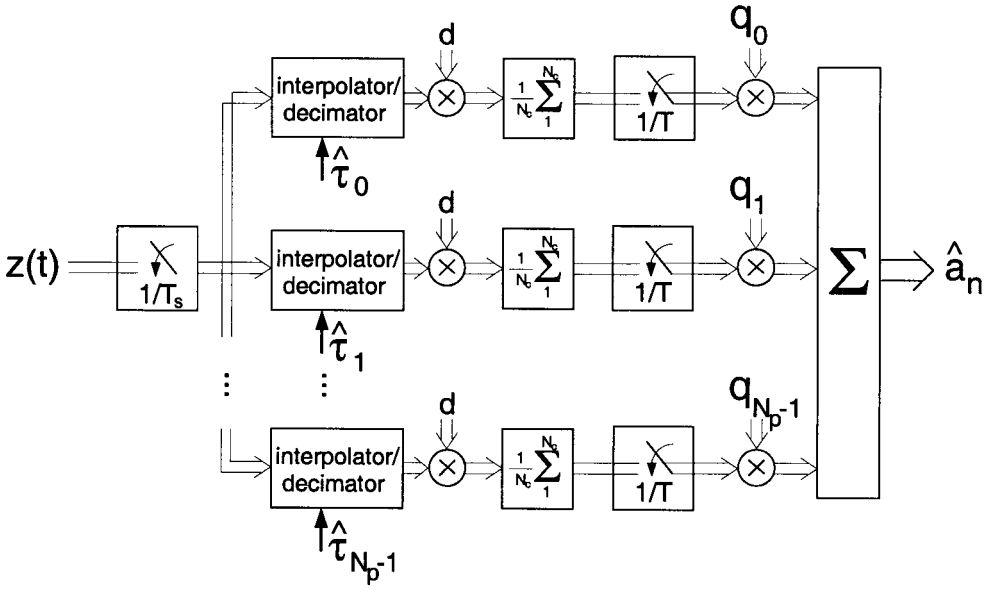

Fig. 1. RAKE receiver model.

transmitter travels through a multipath propagation channel with N_p independent paths (WSSUS model). Each of these paths is characterized by its delay τ_l and fading coefficient c_l

$$h(\tau) = \sum_{l=0}^{N_p-1} c_l(t)\delta(\tau - \tau_l). \tag{2}$$

As the signal enters the receiver, white Gaussian noise $m(t)$ is added

$$r(t) = \sum_{l=0}^{N_p-1} c_l(t) \sum_n a_n \sum_{\nu=0}^{N_c-1} d_{nN_c+\nu} \cdot g_T(t - nT - \nu T_c - \tau_l) + m(t). \tag{3}$$

In the first stage of signal processing in the receiver, the signal is filtered with a filter matched to the pulse-forming filter in the transmitter. Thus, in combination with the following RAKE [1] receiver, a channel matched filter is formed. The signal at the output of the pulse matched filter is given by

$$z(t) = \sum_{l=0}^{N_p-1} c_l(t) \sum_n a_n \sum_{\nu=0}^{N_c-1} d_{nN_c+\nu} \cdot R_g(t - nT - \nu T_c - \tau_l)l + \tilde{m}(t). \tag{4}$$

The noise term $\tilde{m}(t)$ represents both the noise filtered by the pulse matched filter and the interference by other users. Other user interference is modeled as additional noise in order to keep the model simple and highlight the important effects. The combined transmit and receive filter pulse form is denoted by $R_g(t)$, the effective pulse form at the output of the pulse matched filter

$$R_g(t) = \int_{-\infty}^{\infty} g^*(\tau)g(t+\tau)\,d\tau. \tag{5}$$

The matched filter output signal is used as input for the RAKE receiver (see Fig. 1).The RAKE implementation shown here operates on samples from the matched filter output taken at an arbitrary rate $1/T_S$ (at least Nyquist sampling). In each of the M branches of the RAKE, the samples are processed by means of interpolation and decimation [2] in order to obtain intermediate samples $z_{l,k}$ with a rate of $1/T_c$ and to compensate for the delay τ_l. Alternatively, instead of interpolation and decimation, one could adapt the code phases in order to compensate the delays in the individual paths. The time discrete signal inside branch l of the RAKE, just behind the timing compensation, that results from one transmitted symbol can be expressed as

$$\begin{aligned} z_{l,k} = {} & a_n c_{l,n} \cdot \sum_{\nu=0}^{N_c-1} d_{nN_c+\nu} \cdot R_g(kT_c - nT - \nu T_c + \hat{\tau}_l - \tau_l) \\ & + a_n \cdot \sum_{\substack{i=0 \\ i\neq l}}^{N_p-1} c_{i,n} \sum_{\nu=0}^{N_c-1} d_{nN_c+\nu} \\ & \cdot R_g(kT_c - nT - \nu T_c + \hat{\tau}_l - \tau_i) + \tilde{m}_{l,k}. \end{aligned} \tag{6}$$

Since Nyquist pulses are used for transmission, after pulse matched filtering and compensation of the path delay (using the estimate $\hat{\tau}_l$), only one transmitted symbol a_n contributes to the resulting signal originating from path l if perfect timing ($\hat{\tau}_l = \tau_l$) is assumed. As path delay compensation can only be done for one path at the same time, this is not true for the other paths: these additional paths lead to interchip interference (ICI) as well as intersymbol interference (ISI), which is not shown here as only the effect of one transmitted symbol is described. But in this framework, it is sufficient to approximate this effect by an additional noise term contributing to $\tilde{m}_{l,k}$. Furthermore, the fading coefficients $c_l(t)$ are assumed to be constant over one symbol interval and are thus replaced by $c_{l,n}$.

The next step required for detecting the symbol is the despreading. The signal $z_{l,k}$ is now multiplied with the complex conjugate of the spreading sequence $\mathbf{d}^*$ before summing the signal over one symbol period. Therefore, the despread signal, denoted with $y_{l,n}$, simplifies to an expression very familiar to the matched filter output known from traditional (nonspread)

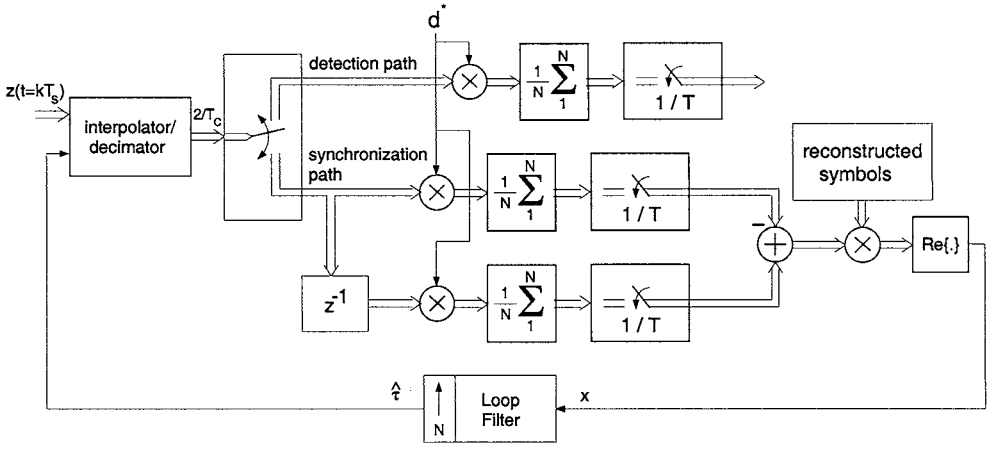

Fig. 2. Conventional coherent EL tracking loop.

frequency-nonselective single-carrier communication systems, apart from some additional unwanted multipath interference

$$\begin{aligned} y_{l,n} &= \frac{1}{N_c}\sum_{k=nN_c}^{(n+1)N_c-1} d_k^* z_{l,k} \\ &= a_n c_{l,n} \\ &\quad + \underbrace{a_n \sum_{i,k,\nu} c_{i,n} d_k^* d_{nN_c+\nu} R_g(kT_c - nT - \nu T_c - \hat{\tau}_l + \tau_i)}_{\text{multipath interference}} \\ &\quad + \acute{m}_{l,n}. \end{aligned} \tag{7}$$

Note that it is assumed here that the number of RAKE fingers and the number of physical multipaths are both given by N_p. The combiner computes a linear combination of the despreader output $y_{l,n}$ by weighting with the combiner coefficients q_l (e.g., $\hat{c}_l^*$ for maximum ratio combining).

To be functional, a RAKE receiver needs estimates for the path delays τ_l and the fading coefficients c_l. The task of the algorithms we are concerned with here is to continuously adapt the estimates $\hat{\tau}_l$ to the true values during normal operation and to provide accurate estimates $\hat{c}_l$ for the fading coefficients. Therefore, each branch of the RAKE has its own timing tracking loop and phasor estimator. Obviously, this algorithmic view may not reflect the actual implementation, which could share such components among several branches.

III. Timing Tracking

A. Conventional TED

The conventional timing error detector often used in CDMA systems is the early–late (EL) timing error detector (see Fig. 2). This timing error detector operates on two classes of samples of the matched filter output: one taken early and one taken late with respect to the detection path. For a good compromise between performance and implementation complexity, the early and late branches are usually spaced half a chip apart ($T_c/2$) from the detection branch. In the case of no timing error, everything is obviously balanced, hence resulting on average in no signal at the output of the timing error detector at all. In the case where the signal is delayed by $T_c/2$, the late branch is perfectly aligned and therefore delivers a large positive output. The output of the overall timing error detector is calculated as the difference between late and early branch outputs. In the aforementioned case, this leads to a positive value at the TED output for positive delays of the signal. In the case of negative delays with respect to the receiver time base, the output becomes negative. The output of the conventional EL-TED is given by

$$\begin{aligned} x &= x(nT) \\ &= Re\left\{ \hat{a}_n^* \hat{c}_n^* \sum_{k=nN_c}^{(n+1)N_c-1} \left(z(kT_c + T_c/2 + \hat{\tau}) \right.\right. \\ &\qquad \left.\left. - z(kT_c - T_c/2 + \hat{\tau}) \right) d_k^* \right\}. \end{aligned} \tag{8}$$

The correlation length N is not necessarily limited to one symbol ($N \neq N_c$) but can be chosen larger if channel coherence time permits. Data symbols $\hat{a}_n$ and phasor estimates $\hat{c}_n$ have to be used with the right time alignment in this case. If we assume a flat fading channel ($N_P = 1$), the output of the timing error detector, conditioned on the fading coefficient and dependent on the uncompensated timing error ($\tau - \hat{\tau}$), is on average given by

$$\begin{aligned} E[x|c] &= Re\{E[|a|^2]|c|^2[R_g(T_c/2 + \hat{\tau} - \tau) \\ &\qquad - R_g(-T_c/2 + \hat{\tau} - \tau)]\} \\ &= E[|a|^2]|c|^2 S(\tau - \hat{\tau}). \end{aligned} \tag{9}$$

The dependence of the average TED output on the residual timing error $\tau - \hat{\tau}$ can be illustrated by the open-loop S-curve $S(\tau - \hat{\tau})$. The conventional TED operates correctly in the case of a flat fading scenario. However, in the case of multipath propagation ($N_P > 1$), the channel model changes, and therefore the output of the TED, conditioned on the set of fading

coefficients $\mathbf{c}$, becomes strongly influenced by the additional multipaths

$$E[x_m|\mathbf{c}] = E[|a|^2]Re\left\{c_m^* \sum_{l=0}^{N_p-1} c_l S(\tau_l - \hat{\tau}_m)\right\} \tag{10}$$

$$= E[|a|^2]Re\{|c_m|^2 S(\tau_m - \hat{\tau}_m)\} \tag{11}$$

$$+ \underbrace{E[|a|^2]Re\left\{c_m^* \sum_{l=0\cdots N_p-1,\, l\neq m} c_l S(\tau_l - \hat{\tau}_m)\right\}}_{\text{low frequency interference}}. \tag{12}$$

The deteriorating effects described in (12) do have a larger impact on the overall system than one might expect from their power compared to the underlying noise processes $\acute{n}_{l,n}$ of similar power. This is the case because these effects originate from the bandlimited fading processes, and therefore are bandlimited to twice the bandwidth of the fading process. The bandwidth of this fading process, on the other hand, is usually much smaller than the overall signal and noise bandwidth, even for large mobile speeds. Therefore, the low-pass filter effect of the timing tracking loop filter will reject significant amounts of noise but cannot be as effective on the low-frequency interference. For a visualization of system performance in the presence of these uncompensated multipath distortions, see Fig. 9. The additional terms (12) can easily degrade the timing tracking in a way that it becomes almost useless and overall system performance is affected severely. For each instance in time, depending on the present constellation of delays and fading coefficients of other paths, the output of the TED appears to be biased. Since the channel is assumed to be fading in the long term, this short-term bias could, for example, be modeled as an increased estimator variance. But for low mobile speeds such an approximation may be misleading, as, due to the biased estimate, the receiver may already lose lock in the meantime. Therefore, averaging is not the method of choice in order to combat these effects.

B. TED Interference Cancellation

As seen above, the TED output in each RAKE finger is influenced by a large amount of interference from the adjacent paths. Fortunately, it is possible to reconstruct the interference, because the fading coefficients and relative delays are already known with sufficient accuracy in tracking mode, and thus cancel it. In doing so, we are able to compute a compensation term that allows us to cancel the effect of other paths on the timing error signal x_m, i.e.,

$$\tilde{x}_m = x_m - Re\left\{\hat{c}_m^* \sum_{l=0\cdots N_p-1,\, l\neq m} \hat{c}_l S(\hat{\tau}_l - \hat{\tau}_m)\right\}. \tag{13}$$

The scheme presented here is not limited by any assumptions made on the minimum spacing of paths [7]. Therefore, it is able to track closely spaced paths well to and below one chip apart. The paths are tracked individually and the tracker will follow each of them correctly if they eventually diverge again. The presented technique is not limited by the fact that it has to focus on the stronger of two paths, as often supposed in heuristic solutions for dealing with this type of scenarios.

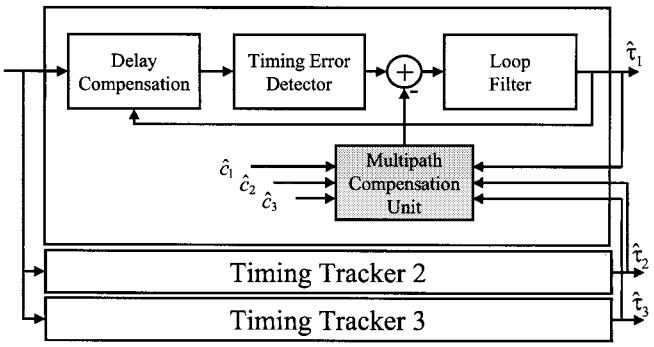

Fig. 3. Structure of cancellation mechanism.

As the new cancellation unit (see Fig. 3) introduces additional complexity, this topic is discussed here briefly: a new compensation value has to be calculated each time the channel scenario changes significantly. This usually equals the rate at which the fading coefficients have to be estimated. The rate at which the canceler updates its compensation values might therefore be well below symbol rate. This reduction in complexity becomes most interesting in the case of slowly moving mobiles in indoor environments with Doppler frequencies of only a few hertz. To further reduce the complexity of this algorithm, the interference canceler could be limited to cancel only the effects of the strongest interfering path.

C. TED Interference Minimization

A different possible extension to the conventional EL scheme is to use more than two samples in order to compute one TED value. A finite impulse response (FIR) filter (see Fig. 4) may be used to accomplish this task. The FIR filter of length L is defined by its coefficients $\boldsymbol{\xi} = [\xi_0 \cdots \xi_{L-1}]$ and delays $\boldsymbol{\delta} = [\delta_0 \cdots \delta_{L-1}]$ relative to the detection path. The expectation of the TED/FIR output, with respect to the channel fading coefficients, can be written as

$$E[x_m|\mathbf{c}] = E[|a|^2] \cdot Re\left\{c_m^* \sum_{l=0}^{N_p-1} c_l \sum_{u=0}^{L-1} \xi_u R_g(\delta_u + \hat{\tau}_m - \tau_l)\right\}. \tag{14}$$

Therefore, the variance of the noise signal superimposed by path l on the TED output of path m, assuming a WSSUS fading, can be approximated ($\hat{\tau} \approx \tau$, $\hat{c} \approx c$) as

$$\tfrac{1}{2}(E[|a|^2])^2 \left|\sum_{u=0}^{L-1} \xi_u R_g(\delta_u + \hat{\tau}_m - \tau_l)\right|^2 E[|c_m|^2]E[|c_l|^2]. \tag{15}$$

It can be seen that the amount of multipath distortion depends on the FIR coefficients that are used. In addition to this multipath distortion, there is the additive white Gaussian noise, which is also filtered by the FIR. Assuming Nyquist pulses and a chip-spaced FIR, the channel noise is amplified by $(1/2)\|\boldsymbol{\xi}\|^2$, thus proportional to the filter energy. Nevertheless, the two noise

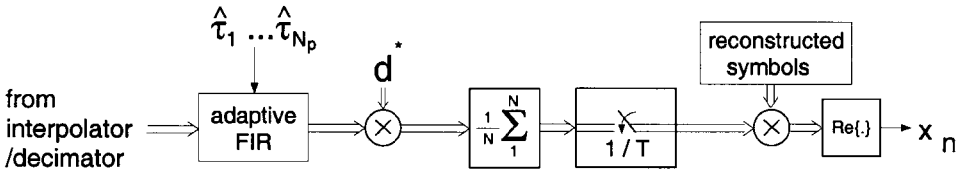

Fig. 4. Adaptive timing error detector.

processes shown above have completely different impact on the performance of the TED in a closed-loop structure. Depending on the loop bandwidth, most of the channel noise is rejected by the loop filter. On the other hand, most of the multipath interference passes the loop filter [see Fig. 5(a)]. Therefore, depending on the loop filter bandwidth and the spectral distribution of the noise processes, both noise terms have to be weighted appropriately. Two possible approaches to determine the FIR coefficients are described in the Appendix: a low complexity approach with certain restrictions and a more general one.

D. Simulation Results for Timing Tracking

The effect of adjacent paths on the open-loop performance is demonstrated in Fig. 5(a). The output of the TED is plotted versus the symbol time index. Depicted is the stronger of the two paths in an indoor scenario ($N_c = 4$) with a mobile speed of 10 km/h. No timing error was present during these simulations. Therefore, an ideal TED would produce no error signal at all. In reality, the raw TED signal is influenced by two terms: a high—frequency noise term (mainly self-noise) and low-frequency adjacent path interference. The self-noise can be suppressed effectively if the TED output is sufficiently low-pass filtered. This is demonstrated for normalized low-pass filter bandwidths of 1/10 and 1/100. For the smallest filter bandwidth, the noise is suppressed almost completely, but the adjacent path interference remains the same. The presented interference cancellation scheme allows one to remove the adjacent path interference without significantly increasing the noise term [Fig. 5(b)]. In combination with additional low-pass filtering, the flat line behavior of the ideal TED without any additional paths is approximated very closely.

To demonstrate the achievable performance gains of the overall system, the new TED schemes have been integrated into a tracking loop inside a RAKE receiver. The simulation setup was compatible with the 3GPP proposal [9]. An indoor scenario with spreading factor $N_c = 4$ and mobile speed $v = 10$ km/h was used. Furthermore, it was assumed that two multipath components, spaced one chip apart, were present, with the average power of the second path 10 dB below the first. Fig. 6(a) shows the estimated delays of the two paths over a simulation interval of 5 s for a conventional EL TED. The original paths are located at 2 (respectively, 3) T_c. The weaker path moves toward the stronger one and merges within a fraction of a second. From that time on, only a combination of both paths is tracked. Even the stronger path is not tracked very well. If the cancellation scheme is active, the cross-effects between the different paths are eliminated almost completely and both paths are tracked almost perfectly [Fig. 6(b)]. Note that only results for the interference minimization scheme are presented, since the results for the interference cancellation

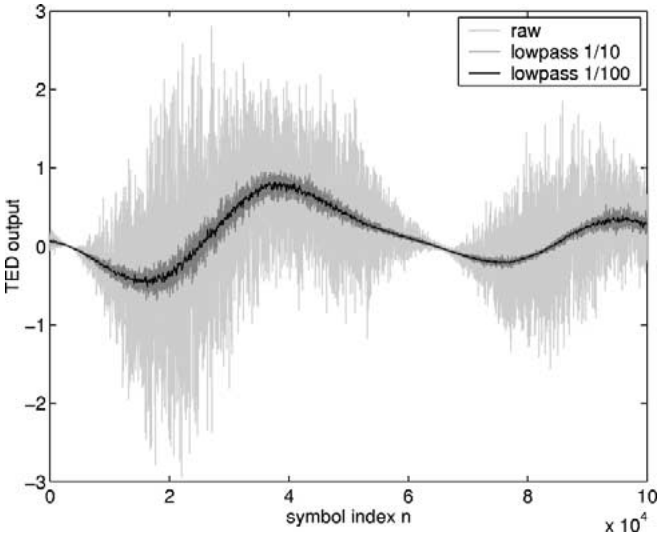

(a)

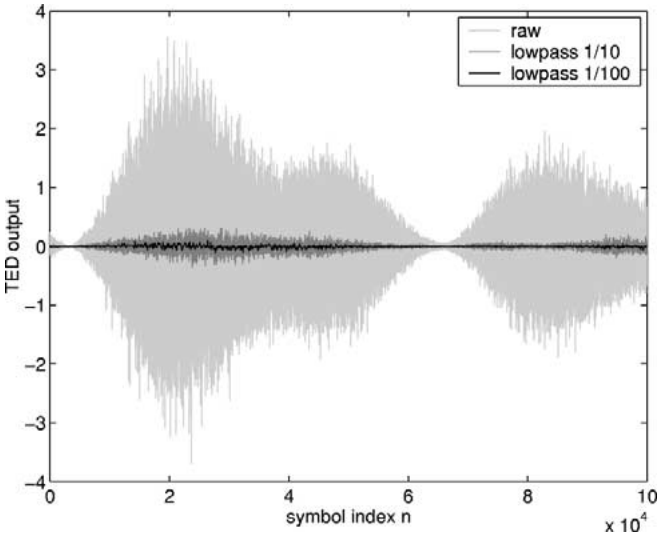

(b)

Fig. 5. Output of TED: (a) standard and (b) with cancellation.

scheme are qualitatively the same. All presented interference cancellation/minimization schemes show similar performance if applied to moderate scenarios. However, the simplified scheme described in Appendix A is mainly suitable for suppressing only one additional path. The extended interference suppression algorithm described in Appendix B is capable of suppressing multiple paths but has to use an FIR filter with a larger number of taps in order to do so. The interference cancellation scheme shows similar or, in some scenarios, slightly better performance but does depend on good channel phasor estimates. These estimates can be provided by the phasor estimation algorithm described in the next section. It

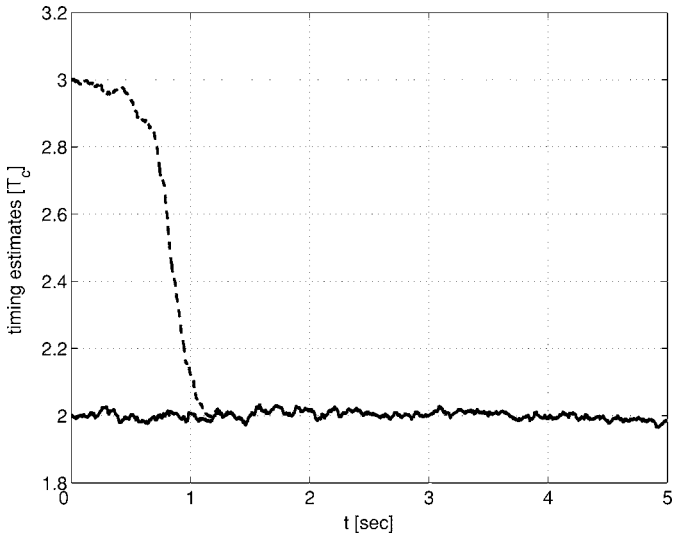

(a)

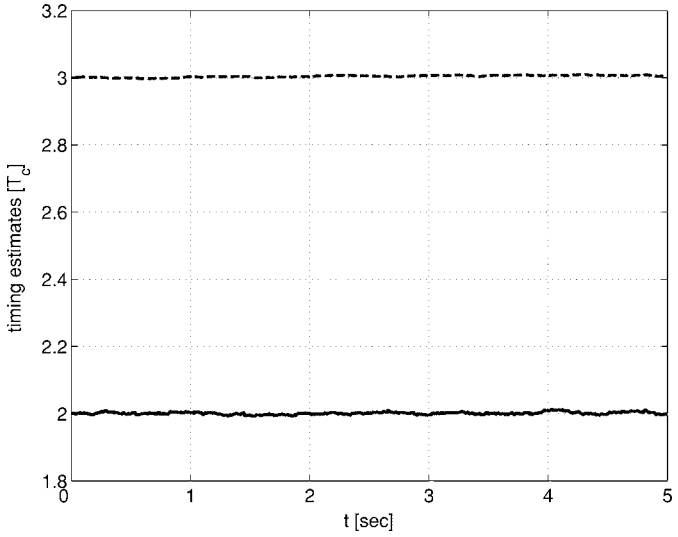

(b)

Fig. 6. Delay estimates ($N_c = 4$): (a) conventional TED and (b) TED with interference min.

delivers estimates of the fading coefficients in such a way that cross-effects between phasor estimation and timing tracking can be neglected.

IV. Phasor Estimation

Based on the transmission model given by (7), the optimal channel estimator is given by the conditional expected value given all available observations $\mathbf{y}$ and the corresponding symbol sequence $\mathbf{a}$

$$\hat{c}_{l,n} = E[c_{l,n}|\mathbf{y}, \mathbf{a}]. \tag{16}$$

In [2], it is shown that this optimal phasor estimate can be generated by low-pass filtering maximum-likelihood (ML) phasor estimates $\hat{\mathbf{c}}_{\mathrm{ML};l}$ with a Wiener filter $\mathbf{w}$ of normalized bandwidth F corresponding to the bandwidth of the Doppler spectrum $S(e^{j\omega})$ of the fading process, i.e., we have that

$$\hat{c}_{l,n} = \mathbf{w}^H \cdot \hat{\mathbf{c}}_{\mathrm{ML};l}. \tag{17}$$

Here, we constrain the Wiener filter to a fixed number of N_w coefficients. The Wiener filter therefore reduces to a single, time-invariant N_w-tap FIR filter $\mathbf{w} = (w_0, w_1, \ldots, w_{N_w-1})^T$. How to obtain the filter tap weights is indicated in Appendix C. In essence, it can be said that the phasor estimation algorithm relies on ML phasor estimates, which are simply postprocessed (filtered) by a fixed FIR filter.

A. Maximum Likelihood Phasor Estimation With Multipath Interference Cancellation

Usually, in a CDMA system the assumption is made that there is no unwanted multipath interference, and in that case the despreader output reduces to

$$y_{l,n} = a_n c_{l,n} + \acute{m}_{l,n}. \tag{18}$$

If this assumption holds, the ML phasor estimates are simply given by [2]

$$\hat{c}_{\mathrm{ML};l,n} = a_n^* \cdot y_{l,n} = c_{l,n} + \breve{m}_{l,n}. \tag{19}$$

However, if multipath propagation is present, the interfering multipaths cannot be neglected. Let us assume that ML phasor estimates are formed using the despreader output of (7) and a simple complex conjugate multiplication with a known symbol a_n. The multipath interference then introduces additional terms in the ML phasor estimate, which is now given by

$$\sum_i R_g(-\tau_l + \tau_i) c_{i,n} + w_{l,n}. \tag{20}$$

The first term is directly dependent on the raised cosine function $g(t)$, the timing delays τ_l, τ_i, and the phasors $c_{i,n}$ of the multipaths. This term includes the desired fading coefficient $c_{l,n}$ for $i = l$. But it also manifests as a systematic error for $i \neq l$, being a random process of bandwidth F given by the Doppler spectrum $S(e^{j\omega})$. This interference cannot be suppressed by the Wiener filter and has to be cancelled beforehand; otherwise, a significant performance degradation of the RAKE receiver may result. If scrambling is applied in addition to spreading, the additional interference $w_{l,n}$ behaves approximately like white Gaussian noise and can be suppressed, at least partially, by the Wiener filter. Therefore, it is now possible to write the ML phasor estimates as follows:

$$\begin{aligned}\hat{c}_{\mathrm{ML};l,n} &= c_{l,n} + \sum_{\substack{i=0 \\ i\neq l}}^{N_p-1} R_g(-\tau_l + \tau_i) c_{i,n} + u_{l,n} \\ &= \sum_{i=0}^{N_p-1} R_g(-\tau_l + \tau_i) c_{i,n} + u_{l,n}\end{aligned} \tag{21}$$

where $u_{l,n} = w_{l,n} + \breve{m}_{l,n}$ is assumed to be AWGN. Rewriting this in matrix form for all RAKE fingers, we get

$$\underbrace{\begin{pmatrix} \hat{c}_{ML;0,n} \\ \vdots \\ \hat{c}_{ML;N_p-1,n} \end{pmatrix}}_{\hat{\mathbf{c}}_{ML;n}} = \mathbf{G} \underbrace{\begin{pmatrix} c_{0,n} \\ \vdots \\ c_{N_p-1,n} \end{pmatrix}}_{\mathbf{c}_n} + \mathbf{u} \tag{22}$$

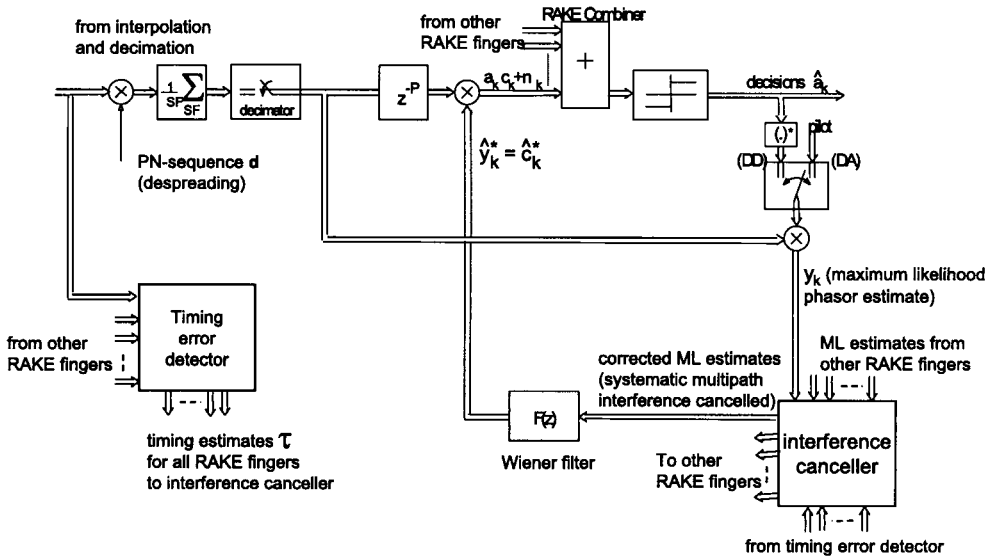

Fig. 7. Phasor estimation for a RAKE receiver.

where the matrix $\mathbf{G}$ is given by

$$\mathbf{G} = \begin{pmatrix} g(\tau_0 - \tau_0) & \cdots & g(\tau_0 - \tau_{N_p-1}) \\ \vdots & \ddots & \vdots \\ g(\tau_{N_p-1} - \tau_0) & \cdots & g(\tau_{N_p-1} - \tau_{N_p-1}) \end{pmatrix}. \quad (23)$$

The minimum mean square error (LMMSE) [3] solution of the interference cancellation problem is thus given by

$$\underbrace{\begin{pmatrix} \hat{c}_{\mathrm{LMMSE};0,n} \\ \vdots \\ \hat{c}_{\mathrm{LMMSE};N_p-1,n} \end{pmatrix}}_{\hat{\mathbf{c}}_{\mathrm{LMMSE}}} = \mathbf{C}_C \mathbf{G}^T (\mathbf{G}^T \mathbf{C}_C \mathbf{G} + N_0 \cdot \mathbf{I})^{-1} \hat{\mathbf{c}}_{ML;n}. \quad (24)$$

Since the N_p fading processes are assumed to undergo mutually uncorrelated scattering, the autocorrelation matrix $\mathbf{C}_C$ can be written as

$$\mathbf{C}_C = \mathrm{diag}(\rho_0 \cdots \rho_{N_p-1}) \quad (25)$$

where ρ_l denotes the average process power of the lth multipath (see also Appendix C). Furthermore, it is noted that knowledge of the multipath delays τ_l, τ_i is required in order to perform the partial interference cancellation. These timing delays can be obtained from the TED described in Section III. The multipath delays $\tau_{l,i}$ are extremely slowly varying processes, and for the purpose of phasor estimation can safely be assumed constants as long as the multipath components are treated appropriately, as described earlier in this paper. The resulting structure for the phasor estimation is shown in Fig. 7. The design of the Wiener filter for the estimator inside a single branch of the RAKE is described in Appendix C.

B. Simulation Results for Phasor Estimation

The performance of the new phasor estimator was evaluated by means of simulation. The simulation setup was as follows. We assumed a UMTS frequency-division duplexing system operating with a spreading factor of $N_c = 4$. The Wiener filter was employed as a one-step predictor with $N_w = 20$ taps. The velocity was chosen to be $v = 250$ km/h. Obviously, such a speed does not make any sense in an indoor scenario, but it helps to speed up simulation times, since the higher velocity makes the fading process much faster, and it still delivers representative results. The channel consisted of two equally strong paths, with a spacing of 0.5 chips at an SNR of 15 dB. Fig. 8 illustrates qualitatively the improvements that are achievable by the new phasor estimation scheme. The smooth lines represent the reference of perfect phasor estimates. The noisy ones represent the estimates. Fig. 8(a) shows the power of the phasor estimates versus time, when interference cancellation is turned off. Clearly, in such a scenario, the multipath interference is too strong and the estimator is not able to follow the true channel. Fig. 8(b) demonstrates that the new phasor estimation scheme employing partial multipath interference cancellation clearly outperforms the old scheme and tracks the true channel well.

V. System Performance Results

Fig. 9 shows the resulting bit error rates (BERs) for the TED using interference cancellation compared to the bound of perfect synchronization and in comparison to a conventional EL-TED with the same loop design. These results were obtained for the channel profile with two paths spaced one chip apart and the second one 10 dB in power below the first one. For the standard TED without cancellation, a BER degradation with resulting SNR losses of several decibels can be observed. These losses are reduced to a fraction of a decibel if the cancellation scheme is active. Differences between the improved TED schemes described above cannot be observed in a graph of this scale and result with proper design only in a fraction of a decibel.

Fig. 10 shows an exemplary simulation result for a RAKE with phasor and timing tracking suitable for environments with closely spaced multipaths. The scenario is the same as before but with a tap spacing of $0.8 \cdot T_c$ and a mobile speed of 120 km/h.

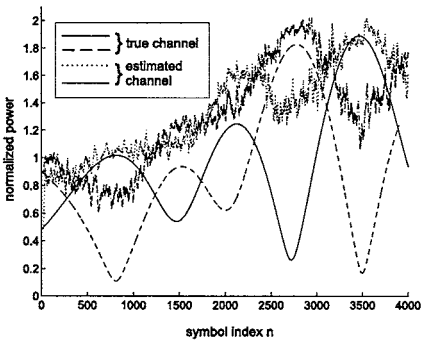

(a)

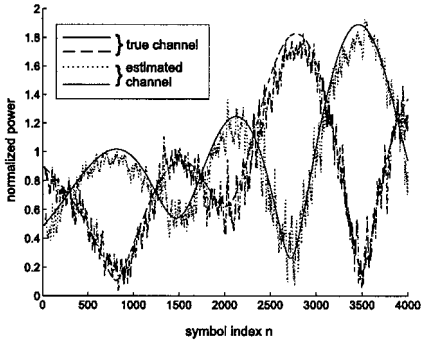

(b)

Fig. 8. Phasor estimation example: (a) without interference cancellation and (b) with interference cancellation.

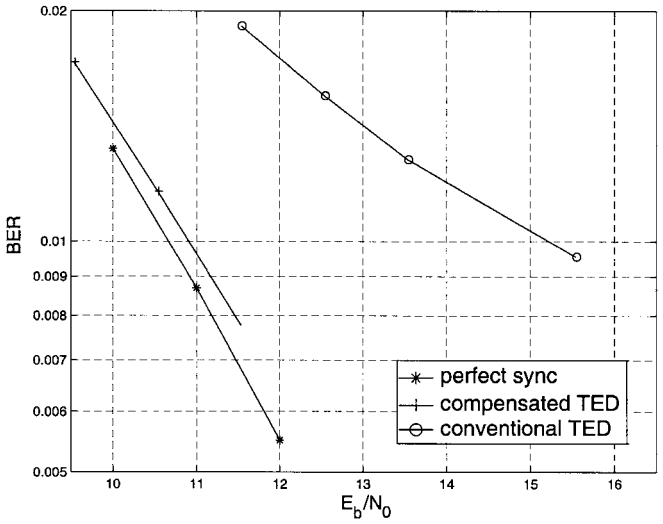

Fig. 9. BER, adaptive code-tracking, $N_c = 4$.

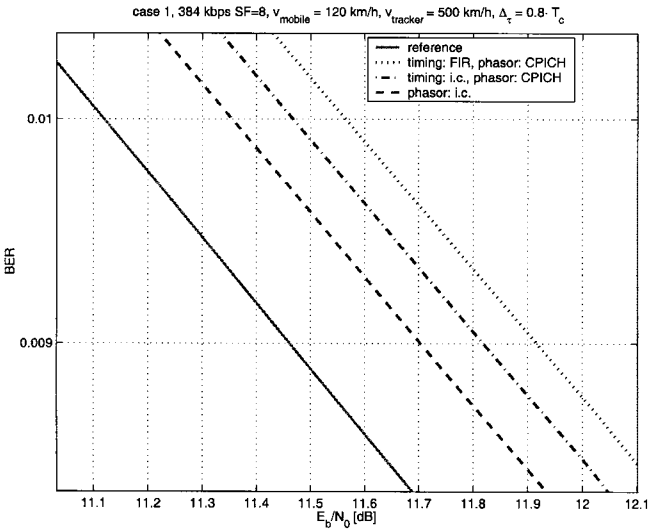

Fig. 10. Overall synchronization performance, 120 km/h.

The leftmost curve is the reference with perfect synchronization. A RAKE without advanced synchronization algorithms, i.e., no interference cancellation or adaptive prefiltering, will lose lock on its fingers very quickly, resulting in an overall SNR loss of more than 4 dB at a target BER of 10^{-2}. The two rightmost curves here depict the performance for phasor tracking with a Wiener interpolator without interference cancellation and with advanced timing tracking. The second curve from the left shows the performance when phasor estimation is performed with interference cancellation, according to Section IV. In this scenario, the overall BER loss was reduced to only 0.2 dB. In general, the advanced algorithms presented here are most effective in scenarios with closely spaced multipath of equal strength. For phasor estimation, the effects are most obvious for spacings of noninteger multiples of the chip duration (especially $0.5T_c$, $1.5T_c$). In such extreme cases, interference cancellation for phasor estimation alone results in performance improvements of several decibels, not just 0.1 dB as shown in Fig. 10.

VI. Conclusion

The effects of multipath propagation on conventional timing error detectors and phasor estimators have been analyzed. This analysis provided the means for the derivation of new algorithms that can cancel out or suppress most of the deteriorating effects of multipath propagation on both timing and phasor estimation. Three possible approaches for the extension of timing tracking to multipath scenarios have been discussed: an interference cancellation approach and two versions of an interference minimization scheme. All three of them achieve comparable performance over a wide range of scenarios. Therefore, the selection of the appropriate one has to be based on the actual scenarios and implementation aspects. Furthermore, to achieve full performance, one of the advanced TEDs has to be combined with the extended phasor estimation.

The new phasor estimation algorithm can also be classified as an interference minimization approach (i.e., it minimizes the low-frequency portion of the multipath interference). Since the calculation of the phasor estimation interference cancellation solution only depends on the very slowly varying timing estimates and the known raised cosine function, it is sufficient to perform calculation of the estimator's coefficients on a very low rate. The interference cancellation scheme for timing tracking has to be adapted with the same low rate and is not critical with respect to processing power either. The coefficients for TED interference minimization schemes only have to be recomputed if the relative path delays change. The phasor estimates are not used for these schemes at all. On the other hand, low-complexity FIR filtering has to be done at chip rate. Therefore, the additional computational effort required for all of the algorithms presented

here is minimal, which makes them ideal for RAKE receivers in the mobile user equipment.

Employing the interference cancellation/minimization schemes extends the field of application for channel estimation to the area of closely spaced propagation delays. The achievable performance gains over the conventional algorithms without compensation schemes were illustrated by means of simulation for a few typical cases. It must be mentioned that the achievable performance gains depend heavily on the scenario and may vary from a few fractions of a decibel to several decibels in terms of BER. Large performance gains are realizable compared to standard single-path algorithms, and the bound of perfect synchronization is approached closely.

APPENDIX A
LOW-COMPLEXITY INTERFERENCE MINIMIZATION

The new code tracking loop includes an adaptive TED that mitigates the effect that adjacent propagation paths have on the error signal of each RAKE finger by prefiltering the signal in the synchronization path. The structure of the TED is shown in Fig. 4. Instead of using a fixed two-tap FIR filter, as in the early–late case ($1-z^{-1}$), an adaptive FIR filter is employed, and its coefficients are updated reflecting the current channel scenario. Consider the expected value of the error signal x (S-curve) for the conventional TED and a flat fading channel, conditioned on the channel phasor c and the estimated phasor $\hat{c}$. Assuming perfect autocorrelation properties of the effective spreading sequence $\mathbf{d}$ and root-raised cosine transmit and receive filters, it can be written as

$$E[x|c,\hat{c}] = E[|a|^2]Re\{c\hat{c}^*[R_g(T_c/2+\hat{\tau}-\tau) - R_g(-T_c/2+\hat{\tau}-\tau)]\}. \quad (26)$$

Imagining one additional path with a delay difference of τ_Δ with respect to the current path, we can either compute a resulting S-curve that will be severely distorted or intuitively assess the paths' contribution to the current RAKE finger. It will be proportional to its power times the square of the value of the S-curve at $\hat{\tau}-\tau=\tau_\Delta$. The basic idea of mitigating adjacent path interference is thus to reshape the flat-fading-equivalent S-curve of the TED so as to shift its zero-crossings to the locations of adjacent paths. If this is achieved, then those paths will not contribute to the error signal of the current RAKE finger *on average*.

If we filter the synchronization path samples with an FIR filter $\boldsymbol{\xi}=[\xi_0\cdots\xi_{L-1}]$, instead of using the early–late structure, the S-curve for the flat fading case becomes

$$E[x|c,\hat{c}] = E[|a|^2]Re\left\{c\hat{c}^*\sum_{u=0}^{L-1}\xi_u R_g(\delta_u+\hat{\tau}-\tau)\right\} \quad (27)$$

with $\boldsymbol{\delta}=[\delta_0\cdots\delta_{L-1}]$ being the filter tap locations with respect to the detection path samples (i.e., for the EL-TED, we have $\boldsymbol{\delta}=[T_c/2,\ -T_c/2]$). If we assume symmetrical FIR filters in the sense that there are equally many "early" and "late" taps, the following relation holds:

$$\delta_u = \left[\frac{L-1}{2}-u\right]T_c. \quad (28)$$

In this paper, we shall consider a symmetric FIR filter with four taps as a straightforward extension to the conventional TED: $\boldsymbol{\xi} = [-\lambda,\ 1,\ -1,\ \lambda]$ and $\boldsymbol{\delta} = [3T_c/2,\ T_c/2,\ -T_c/2,\ -3T_c/2]$. This leaves us with one design parameter—the outer tap magnitude λ—and thus with one zero-forcing condition for one adjacent path. Inserting $\boldsymbol{\xi}$ and $\boldsymbol{\delta}$ into (27), setting it to zero for $\hat{\tau}-\tau=\tau_\Delta$ and solving for λ yields

$$\lambda(\tau_\Delta) = \frac{R_g(-T_c/2+\tau_\Delta)-R_g(T_c/2+\tau_\Delta)}{R_g(-3T_c/2+\tau_\Delta)-R_g(3T_c/2+\tau_\Delta)}. \quad (29)$$

This characteristic, which is fixed once the FIR structure is known, can be stored in memory and the outer FIR taps can be modified online, depending on the current adjacent path locations. Different resulting S-curves for the chosen FIR structure are shown in Fig. 11 for $\tau_\Delta = 0.9\cdot T_c$, $1.0\cdot T_c$, and $2.0\cdot T_c$. It is noted that for the conventional TED ($\lambda=0$), $\tau_\Delta = 1.5T_c$. For values of τ_Δ smaller than those shown in this figure, the filter energy of the resulting FIR is increased significantly compared to the conventional EL-TED, and noise or additional paths that are present lead to performance degradations. Values of τ_Δ around 0.5 and below cannot be covered with this scheme. The constrained FIR optimization scheme, described in the next section, can be used even in such extreme scenarios. Additional undetected paths may be covered by selecting a lower design SNR in order to make that scheme more robust.

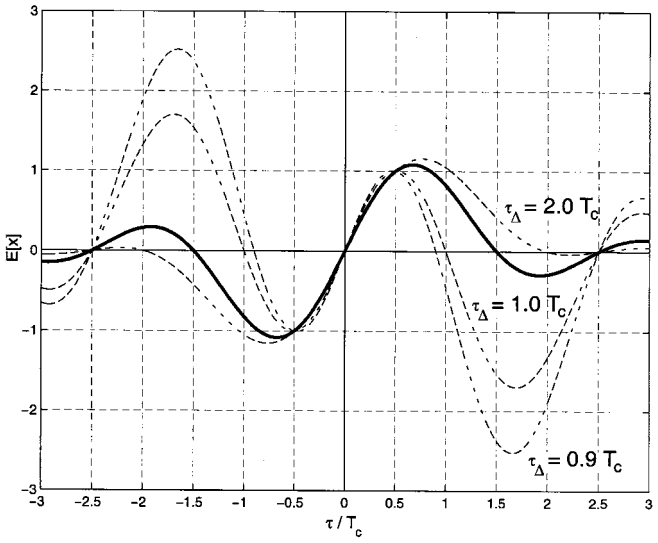

Fig. 11. S-curves for adaptive TED.

APPENDIX B
CONSTRAINED TED FIR OPTIMIZATION

For the new adaptive TED, one possibility of computing filter coefficients is to perform a constrained optimization, where the constraints are given by:

1) zero crossing of S-curve at $\hat{\tau} = \tau$;
2) slope of S-curve normalized at $\hat{\tau} = \tau$.

A first approach would now be to minimize the MSE $E[|x(\hat{\tau} = \tau)|^2]$ of the TED for the case $\hat{\tau} = \tau$ under these constraints. This approach would be correct if there was no further postprocessing of the TED signal. But this signal is further postprocessed by the loop filter, which has a low-pass characteristic. The distortions observed at the TED output are not white but consist, on one hand, of slowly varying components [see (15)] whose bandwidth is limited to twice the Doppler frequency spread. In addition to these low-frequency terms, a white noise term can be observed at the TED output that depends on the noise level at the input of the TED and on the selection of the FIR coefficients. Therefore, as the distortions that finally influence system performance are only those that pass the loop filter, the relative bandwidth of these distortions determines the relative amount of these distortions passing the loop filter. The effective MSE will depend on the length of the FIR filter L on the amount and location of the other paths and on the Doppler frequency spread. For general references on optimization, see [10] and [11].

To minimize the MSE, a cost function $V(\boldsymbol{\xi})$ is defined

$$V(\boldsymbol{\xi}) = \|\mathbf{A}\boldsymbol{\xi}\|^2 + \|\boldsymbol{\xi}\|^2 = \boldsymbol{\xi}^{\mathbf{T}}(\mathbf{A}^{\mathbf{T}}\mathbf{A} + \mathbf{I})\boldsymbol{\xi} \tag{30}$$

where the matrix $\mathbf{A}$ is $(N_p \times L)$ and contains the mean-square contribution of each path at each FIR filter tap location

$$\mathbf{A} = \begin{pmatrix} A_{1,1} & \cdots & A_{1,L} \\ \vdots & \ddots & \vdots \\ A_{N_p,1} & \cdots & A_{N_p,L} \end{pmatrix}$$

$$A_{n,l} = \sqrt{\gamma w E[|c_n|^2]}\, R_g(\delta_l + \hat{\tau}_m - \tau_n). \tag{31}$$

The overall SNR is given by γ, with the coefficients c being normalized to this SNR, and w is the appropriate weighting factor that reflects the different noise attenuation for multipath distortions and channel noise depending on the Doppler spread. τ and δ are normalized to the chip duration T_c. The $(L \times L)$ identity matrix is denoted by $\mathbf{I}$. The aim is now to minimize $V(\boldsymbol{\xi})$, subject to the constraints mentioned above

$$\min_{\boldsymbol{\xi}}\{V(\boldsymbol{\xi})\colon \mathbf{D}\boldsymbol{\xi} = \mathbf{f}\} = \min_{\boldsymbol{\xi} \in F} V(\boldsymbol{\xi})$$
$$\text{s.t.} \quad F = \mathbf{D}^{+}\mathbf{f} + N[\mathbf{D}]. \tag{32}$$

The matrix $\mathbf{D}$ is $(2 \times L)$ and contains the expression for the zero crossing of the TED characteristic at $\hat{\tau} - \tau = 0$ and its slope at the same location

$$\mathbf{D} = \begin{pmatrix} D_{1,1} & \cdots & D_{1,L} \\ D_{2,1} & \cdots & D_{2,L} \end{pmatrix}$$

$$D_{1,j} = R_g(t = \delta_j) \tag{33}$$

$$D_{2,j} = \frac{\partial}{\partial t} R_g(t)\bigg|_{t=\delta_j}. \tag{34}$$

If the slope at the origin is normalized to one, $\boldsymbol{f} = [0\ 1]^T$ describes the two conditions. $\mathbf{D}^{+}$ is the pseudoinverse of $\mathbf{D}$ and $N[\mathbf{D}]$ is its nullspace. The idea is now to move from a constrained optimization to an unconstrained one. To that end, the first step is to reduce the dimensionality of the problem. A singular value decomposition of $\mathbf{D}$ yields

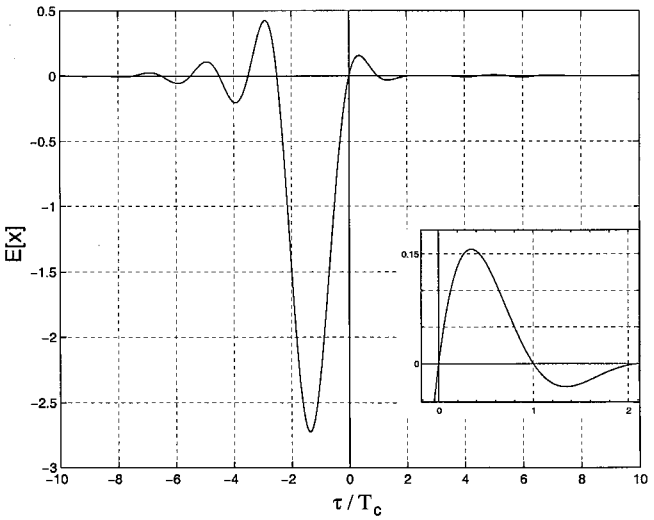

Fig. 12. S-Curve for MMSE adaptively optimized FIR.

$$\mathbf{D} = \mathbf{P}\mathbf{S}\mathbf{Q}^{\mathbf{T}} \tag{35}$$

where $\mathbf{P}$ is (2×2) and $\mathbf{Q}$ is $(L \times L)$. The nullspace of $\mathbf{D}$ is equal to the range of a matrix $\mathbf{H}$, defined as

$$\mathbf{H} = [\mathbf{q}_{\nu+1} \cdots \mathbf{q}_L] \tag{36}$$

with $\mathbf{q}_i$ being the indexed columns of $\mathbf{Q}$ starting from $\nu+1$ with ν defined as the number of eigenvalues. This identity yields the new unconstrained optimization problem

$$\min_{\boldsymbol{\theta} \in R^{L-\nu}} V(\mathbf{D}^{+}\mathbf{f} + \mathbf{H}\boldsymbol{\theta}). \tag{37}$$

Solving for $\boldsymbol{\theta}$ finally yields

$$\boldsymbol{\theta} = -\mathbf{C}^{+}\mathbf{B} \tag{38}$$

with

$$\mathbf{B} = (2\mathbf{f}^{\mathbf{T}}(\mathbf{D}^{+})^{\mathbf{T}}(\mathbf{A}^{\mathbf{T}}\mathbf{A} + \mathbf{I})\mathbf{H})^{\mathbf{T}}$$
$$\mathbf{C} = 2\mathbf{H}^{\mathbf{T}}(\mathbf{A}^{\mathbf{T}}\mathbf{A} + \mathbf{I})\mathbf{H}.$$

The FIR filter $\boldsymbol{\xi}$ is then given by $\boldsymbol{\xi} = \mathbf{D}^{+}\mathbf{f} + \mathbf{H}\boldsymbol{\theta}$. An example for a resulting S-curve in this case is shown in Fig. 12. Here, three paths have been assumed at relative delays of $\tau_1 = 0$, $\tau_2 = T_c$ and $\tau_3 = 2T_c$, with root-mean-square powers of 0, -10, and -20 dB, respectively. It is easily seen that the contributions of the two paths adjacent to that at the origin are nulled out by the zero crossings of the S-curve at their respective locations.

APPENDIX C
SINGLE PATH PHASOR ESTIMATION

1) Channel Dynamics: The time-variant fading coefficients $\{c_{l,n}\}$ are complex-valued random processes. The random fading process is assumed to be wide-sense stationary (WSS), i.e., this process is sufficiently characterized by its mean and covariance. Furthermore, the N_p fading processes are assumed to undergo mutually uncorrelated scattering (US), which is

plausible since individual paths can often be attributed to distinct physical scatterers. The power spectral density $S(e^{j\omega})$ of a fading coefficient $c_{l,n}$ is given by the so-called Jakes spectrum. It is strictly bandlimited to the (normalized to symbol rate) Doppler frequency F and its autocorrelation is denoted with R

$$F = f_0 \cdot \frac{v}{c} \cdot T \tag{39}$$

$$S(e^{j\omega}) = \rho_l \cdot \begin{cases} \dfrac{1}{\pi F} \cdot \dfrac{1}{\sqrt{1-\left(\dfrac{\omega}{2\pi F}\right)^2}}, & \text{for } |\omega| \le 2\pi F \\ 0, & \text{otherwise} \end{cases} \tag{40}$$

$$R(n) = \rho_l \cdot J_0(2\pi F \cdot n) = \rho_l \cdot \alpha(n). \tag{41}$$

In the above equation, ρ_l is the average process power of the lth path, f_0 is the carrier frequency, c is the speed of light, v is the velocity of the mobile handset, and $J_0(\cdot)$ is the Bessel function of the first kind of order zero.

2) Wiener Filtering: The resulting structure for phasor estimation is illustrated in Fig. 7. The required known symbols a_n^* are generated either by forming hard decisions after the RAKE combiner or by inserting known pilot symbols. The ML phasor estimates are postprocessed by the interference canceler, before they are filtered with the Wiener filter. The interference canceler obtains delay estimates from the TED. The corresponding Wiener filter is denoted in the illustration with $F(z)$. The Wiener phasor estimator is identical in form to the LMMSE [3] estimator. In [2], it is shown that the estimator and the corresponding MMSE are given by

$$\hat{c}_n = \underbrace{\mathbf{c}_D^H \cdot (\mathbf{C}_D + N_0 \cdot \mathbf{I})^{-1}}_{\mathbf{w}^H} \cdot \underbrace{\begin{pmatrix} \hat{c}_{LMMSE,\, n-N_w+P} \\ \vdots \\ \hat{c}_{LMMSE,\, n-1+P} \end{pmatrix}}_{\hat{\mathbf{c}}_{LMMSE}}$$

$$\sigma^2_{c;W} = \mathbf{w}^H(\mathbf{C}_D + N_0 \cdot \mathbf{I})\mathbf{w} - \mathbf{w}^H\mathbf{c}_D - \mathbf{c}_D^H\mathbf{w} + \rho \tag{42}$$

where

$$\mathbf{C}_D = \rho \cdot \begin{pmatrix} \alpha(0) & \cdots & \alpha(N_w-1) \\ \vdots & \ddots & \vdots \\ \alpha(N_w-1) & \cdots & \alpha(0) \end{pmatrix} \tag{43}$$

$$\mathbf{c}_D = \rho \cdot (\alpha(N_w-1-P) \cdots \alpha(1-P))^T \tag{44}$$

are the channel tap autocorrelation matrix and the vector of channel tap autocorrelation samples. Note that the factors $\alpha(m) = J_0(2\pi F m)$ in (43) and (44), and the associated channel autocorrelation function, depend on the normalized Doppler shift F. The variable P indicates whether the estimator works as a predictor or a smoother. For $P > 0$, we have a Wiener smoother, which requires the knowledge of future ML phasor estimates. These future estimates can be obtained only if a corresponding delay is introduced between the demodulator for the common pilot channel and the data stream [12].

REFERENCES

[1] R. Price and P. E. Green, Jr., "A communication technique for multipath channels," *Proc. IRE*, Mar. 1958.

[2] H. Meyr, M. Moeneclaey, and S. Fechtel, *Digital Communication Receivers: Synchronization, Channel Estimation and Signal Processing*. New York: Wiley, 1998.

[3] S. M. Kay, *Fundamentals of Statistical Signal Processing—Estimation Theory*. Englewood Cliffs, NJ: Prentice-Hall, 1993.

[4] W. H. Sheen and G. L. Stüber, "Effects of multipath fading on delay locked loops for spread spectrum systems," *IEEE Trans. Commun.*, vol. 42, pp. 1947–1956, Feb. 1994.

[5] W. H. Sheen and C. H. Tai, "A noncoherent tracking loop with diversity and multipath interference cancellation for direct-sequence spread-spectrum systems," *IEEE Trans. Commun.*, vol. 46, pp. 1516–1524, Nov. 1998.

[6] R. D. J. Van Nee, "The multipath estimating delay locked loop," in *Proc. ISSSTA 92*, 1992.

[7] V. Aue and G. P. Fettweis, "A noncoherent tracking scheme for the RAKE receiver that can cope with unresolvable multipath," in *Proc. Int. Conf. Communications*, Vancouver, Canada, 1999.

[8] 3GPP Technical Specification Group Radio Access Network, "Physical layer—General description,", 3G TS 25.201 version 3.0.0.

[9] ——, "Spreading and modulation (FDD),", 3G TS 25.213 version 3.0.0, Oct. 1999.

[10] D. G. Luenberger, *Optimization by Vector–Space Methods*. New York: Wiley, 1969.

[11] R. Fletcher, *Practical Methods of Optimization*. New York: Wiley, 1987.

[12] J. Baltersee, G. Fock, P. Schulz-Rittich, and H. Meyr, "Performance analysis of phasor estimation algorithms for a FDD-UMTS RAKE receiver," in *Proc. ISSSTA 2000*, Parsippany, NJ, Sept. 2000.

[13] H. Boujema and M. Siala, "Enhanced coherent delay tracking for direct sequence spread spectrum systems," in *Proc. ISSSTA 2000*, Parsippany, NJ, Sept. 2000.

[14] G. Fock, P. Schulz-Rittich, J. Baltersee, and H. Meyr, "Multipath resistant coherent timing-error-detector for DS-CDMA applications," in *Proc. ISSSTA 2000*, Parsippany, NJ, Sept. 2000.

[15] P. Schulz-Rittich, G. Fock, J. Baltersee, and H. Meyr, "Low complexity adaptive code tracking with improved multipath resolution for DS-CDMA communications over fading channels," in *Proc. ISSSTA 2000*, Parsippany, NJ, Sept. 2000.

[16] J. Hasson and B. Z. Bobrovsky, "A novel selective combining demodulator for unresolvable multipath in DS-SpSp," in *Proc. VTC 2001*, Rhodes, Greece, May 2001.

Gunnar Fock received the Dipl.-Ing. degree in electrical engineering from Aachen University of Technology (RWTH Aachen), Germany, in 1996, where he is currently pursuing the Ph.D. degree.

Currently, he is a Research Assistant with the Institute for Integrated Signal Processing Systems (ISS), RWTH Aachen. His current research interests include information theoretic aspects of MIMO systems and digital receiver design with emphasis on synchronization, estimation, and equalization.

Jens Baltersee received the M.Eng. degree in electrical and electronic engineering from Imperial College of Science, Technology, and Medicine, London, U.K., in 1996. He is currently pursuing the Ph.D. degree at the Institute for Integrated Signal Processing Systems (ISS), Aachen University of Technology, Aachen, Germany.

He is a Research Assistant at ISS. His current research interests include information theoretic aspects of space–time processing, and digital wireless receiver design with emphasis on synchronization and detection.

Peter Schulz-Rittich received the Dipl.-Ing. degree in electrical engineering from Aachen University of Technology (RWTH Aachen), Germany, in 1998, where he is currently pursuing the Ph.D. degree.

His current research interests include digital receiver design with emphasis on synchronization, channel estimation, and equalization.

Heinrich Meyr (M'75–SM'83–F'86) received the M.S. and Ph.D. degrees from ETH Zürich, Switzerland.

He spent more than 12 years in various research and management positions in industry before accepting a professorship in electrical engineering at Aachen University of Technology (RWTH Aachen) in 1977. He has worked extensively in the areas of communication theory, synchronization, and digital signal processing for the last 30 years. His research has been applied to the design of many industrial products. At RWTH Aachen he heads an institute involved in the analysis and design of complex signal-processing systems for communication applications. He was a Cofounder of CADIS GmbH (acquired in 1993 by Synopsys, Mountain View, CA). He is currently serving on the board of two companies in the communications industry. Recently, he was also appointed as a Member of the Technical Advisory Board of MorphIC's, Cupertino, CA. He has published numerous IEEE papers and holds many patents. He is a coauthor (with G. Ascheid) of *Synchronization in Digital Communications* (New York: Wiley, 1990) and (with M. Moeneclaey and S. Fechtel) of *Digital Communication Receivers. Synchronization, Channel Estimation, and Signal Processing* (New York: Wiley, 1997). In 1998, he was a Visiting Scholar at the University of California (UC) at Berkeley Wireless Research Centre (BWRC).

Dr. Meyr was the "Mc Kay Distinguished Lecturer" of the Electrical Engineering Department of UC Berkeley in spring 2000. He received the "Mannesmann Innovation Prize" in 2000 for outstanding contribution to the area of wireless communication. He was Vice President for International Affairs of the IEEE Communications Society.